



# Temperature-insensitive optical fiber sensor based on SMF-NCF-FMF-NCF-SMF spindle-shaped structure for refractive index measurement

Lei Jing<sup>1</sup> · Haozheng Yu<sup>1</sup> · Zhengrong Tong<sup>1</sup> · Weihua Zhang<sup>1</sup> · Yipeng Tao<sup>1</sup> · Jinlin Mu<sup>1</sup>

Received: 23 January 2024 / Accepted: 22 July 2024 / Published online: 3 August 2024  
© The Author(s), under exclusive licence to Springer-Verlag GmbH Germany, part of Springer Nature 2024

## Abstract

A spindle-shaped sensor with temperature insensitivity based on single-mode fiber (SMF) - no-core fiber (NCF) - few-mode fiber (FMF) - NCF - SMF (SNFNS) for refractive index is proposed. An interferometer with SNFNS structure can be formed by fusing, and then the fiber can be shrunk to form a spindle shape through burning, which is known as an SNFNS spindle-shaped sensor. The introduction of NCF and curvature causes partial light transmitted in the core to enter the cladding, which results in the emergence of phase differences. The interference dips formed by modal interference have different sensitivities to the outside refractive index. The experimental results show that the maximum refractive index sensitivity of sensors is 258.5 nm/RIU in the range of 1.333–1.365. And the sensors have the characteristic of temperature insensitivity in the range of 10–70°C. Accordingly, the proposed sensors are ideal for applications in biomedicine, environment monitoring and other fields.

## 1 Introduction

The advent of optical fiber has caused extensive exploration by scientific researchers. Optical fiber sensors for sensing measurement also emerge at the historic moment. In addition to single-mode fiber (SMF), a variety of special fibers emerge endlessly, such as hollow fiber (HF) [1], photonic crystal fiber (PCF) [2], plastic optical fiber (POF) [3], few-mode fiber (FMF) [4]. Through the research, it is found that heterogeneous sensors with different structures can be prepared by changing the configurations of fibers. These configurations include core-offset [5], taper [6], D-shape [7] and so on. This greatly enriches the variety of optical fiber sensors. For example, there are sensors such as a core-offset Mach-Zehnder interferometer (MZI) [8], a tapered Michelson Interferometer (MI) based on SMF [9], a metal-coated surface plasmon resonance (SPR) sensor with V-shaped grooves [10]. Moreover, the optical fiber sensor can sense a wide variety of physical parameters, such as liquid level

[11], refractive index (RI) [12], micro-displacement [13], gas concentration [14]. The emergence of these sensors has greatly fulfilled multiple needs in various fields. With the superiorities of simple mechanism, small dimension and strong anti-electromagnetic interference ability [15, 16], optical fiber sensors have potential application prospects in medical imaging, biomedicine, aerospace and other fields.

RI can be used to reflect a change in the liquid, which highlights the importance of sensing RI. At present, multitudinous optical fiber sensors for RI sensing have been proposed. In 2018, Liu et al. proposed a core-offset sensor based on erbium-doped fiber. The highest RI sensitivity is -74.22 nm/RIU in the range of 1.333–1.361, which can be obtained without temperature crosstalk. This result is attributed to the introduction of the common difference compensation method [17]. In 2019, Gao et al. proposed a tapered MZI with two waists based on PCF. The results of experiment indicate that in the range of 1.3374–1.3477, the highest RI sensitivity is 263.5 nm/RIU. This sensor achieves sensitivity enhancement by changing the fiber into a tapered shape [18]. Furthermore, the researchers have found that the RI sensitivity can be improved by curving the fiber. Many sensors with curved structures have been proposed. In 2016, Liu et al. proposed a balloon-shaped sensor formed by SMF. The highest RI sensitivity is 225.95 nm/RIU in the range of 1.3493–1.3822. The preparation of the sensor is extremely simple, which can be obtained without splicing and other

✉ Zhengrong Tong  
tjtongzhengrong@163.com

<sup>1</sup> Engineering Research Center of Optoelectronic Devices and Communication Technology, Tianjin Key Laboratory of Film Electronic and Communication Devices, School of Integrated Circuit Science and Engineering, Ministry of Education, Tianjin University of Technology, Tianjin 300384, China

**Table 1** Basic parameters of optical fibers

| Type                              | Value/ $\mu\text{m}$ |
|-----------------------------------|----------------------|
| The core/cladding diameter of SMF | 8.2/125.0            |
| The core/cladding RI of SMF       | 1.4502/1.4450        |
| The cladding diameter of NCF      | 125.0                |
| The cladding RI of NCF            | 1.444                |
| The core/cladding diameter of FMF | 18.5/125.0           |
| The core/cladding RI of FMF       | 1.46111/1.45601      |

methods [19]. In 2021, Wu et al. proposed a curved core-off-set sensor cascaded a fiber Bragg grating (FBG). The results of experiment indicate that in the range of 1.333–1.373, the highest RI sensitivity is -115.5646 nm/RIU. The sensor achieves simultaneous measurement of temperature and RI by cascading FBG [20].

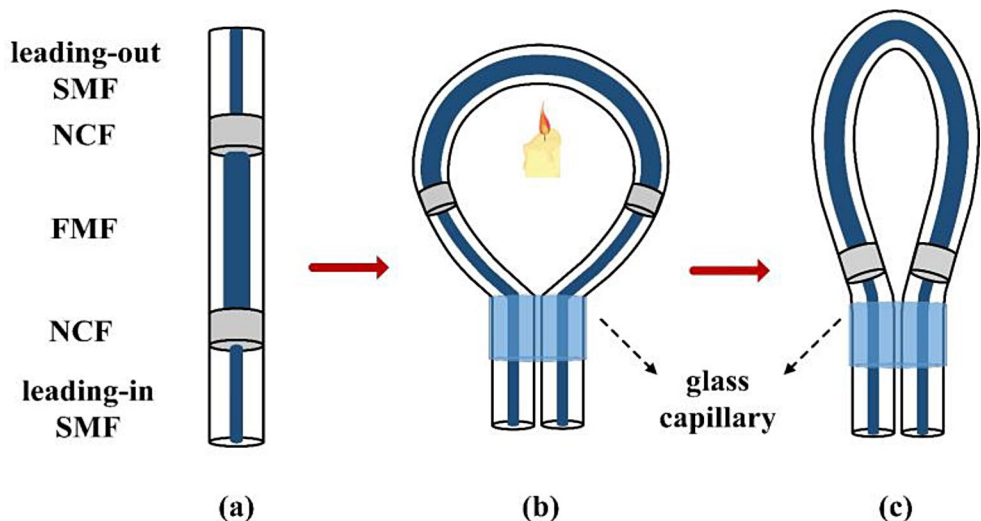
In the study, a spindle-shaped sensor based on SMF-no-core fiber (NCF)-FMF-NCF-SMF (SNFNS) is presented. The sensor can be obtained by fusing SMF, NCF, FMF of different lengths successively and burning the fiber to curve into a spindle shape. The light transmitted in the cladding can excite higher-order modes and interfere with the light transmitted in the core. The different dips generated by different modal interference have different properties. These interference dips have different sensitivity to external RI changes. Compared with the straight SNFNS sensor, the introduction of curvature allows the spindle-shaped sensor to realize the increased sensitivity to RI.

## 2 Theoretical and simulation analysis

### 2.1 The sensor structure and preparation

There are three different fibers, SMF, NCF and FMF, which are used to design and fabricate the SNFNS spindle-shaped sensor. Table 1 presents the basic parameters of three fibers.

**Fig. 1** The preparation of the SNFNS spindle-shaped sensor: (a) SNFNS straight structure (b) SNFNS balloon-like structure (c) SNFNS spindle-shaped structure



As shown in Fig. 1, the preparation of the SNFNS spindle-shaped sensor is roughly divided into three processes. Firstly, SMF, NCF, FMF, NCF, and SMF are fused in sequence by the optical fiber fusion splicer (S178C, Fitel) to form an SNFNS straight structure interferometer. Secondly, the fiber is curved by applying force to form a balloon-like structure. A glass capillary, whose length is 2 cm, is used to regulate the shape of the sensor. Finally, the means of burning fiber with candle flame is used to curve fiber to form an SNFNS spindle-shaped interferometer, which schematic diagram is displayed in Fig. 2(a). And  $d$  denotes the transverse diameter. As the chart shows, light is imported from leading-in SMF core. In NCF, the light is divided into multiple beams that enter the core and cladding of FMF. As the FMF is curved, a small amount of light transmitted in the FMF core enters the cladding. When the light is transmitted to another curved part, most light in the cladding is coupled back into the core. The glass capillary is used to regulate the transverse diameter of the sensor. The actual image of the SNFNS spindle-shaped sensor prepared in the experimentation is shown in Fig. 2(b).

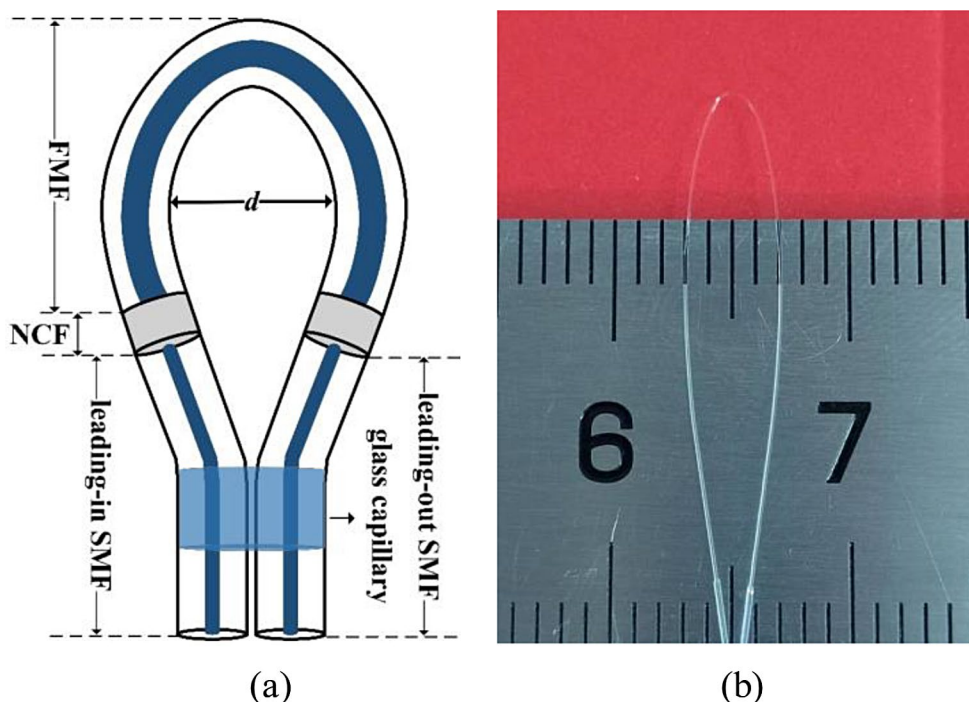
### 2.2 Principle analysis

In SNFNS spindle-shaped sensor, the output light intensity of modal interference can be written as [21]:

$$I = I_1 + \sum_{k=1}^n I_2^k + 2 \sum_{k=1}^n \sqrt{I_1 I_2^k} \cos(\Delta\varphi^k) = I_1 + \sum_{k=1}^n I_2^k + 2 \sum_{k=1}^n \sqrt{I_1 I_2^k} \cos\left[\frac{2\pi L(n_{core} - n_{clad}^k)}{\lambda}\right] \quad (1)$$

where  $I_1$  represents the intensity of mode in core and  $I_2^k$  represents the intensity of  $k$ -order mode in cladding. The phase difference between the mode in core and the  $k$ -order mode in cladding is represented by  $\Delta\varphi^k$ .  $\lambda$  represents the

**Fig. 2** SNFNS spindle-shaped sensor: (a) schematic diagram and (b) actual image



free-space wavelength of input light.  $L$  denotes the sensing length of the sensor. And  $n_{\text{core}}$  and  $n_{\text{clad}}^k$  represent the effective refractivity of the mode in the core and the  $k$ -order mode in the cladding, respectively. According to the Eq. (1) and these parameters, the wavelength of interference dip can be expressed as:

$$\lambda_{\text{dip}} = \frac{2L(n_{\text{core}} - n_{\text{clad}}^k)}{2m + 1} \tag{2}$$

where  $m=0, 1, 2, \dots$ , which is a positive integer. However, modal interference can occur only if the phase difference meets the particular condition, that is,

$$\Delta\varphi^k = (2m + 1)\pi$$

.Therefore, as the RI of the external solution changes, the drift of the interference dip can be expressed as:

$$\frac{\partial\lambda_{\text{dip}}}{\partial RI} = \frac{1}{n_{\text{core}} - n_{\text{clad}}^k} \frac{\partial(n_{\text{core}} - n_{\text{clad}}^k)}{\partial RI} \lambda_{\text{dip}} \tag{3}$$

And as the temperature of the ambient environment changes, the drift of the interference dip can be expressed as [22]:

$$\frac{\partial\lambda_{\text{dip}}}{\partial T} = \left(\alpha + \frac{\xi_{\text{core}} n_{\text{core}} - \xi_{\text{clad}} n_{\text{clad}}^k}{n_{\text{core}} - n_{\text{clad}}^k}\right) \lambda_{\text{dip}} = (\alpha + \Delta n_{\xi}) \lambda_{\text{dip}} \tag{4}$$

where  $\alpha$  denotes the thermal expansion coefficient of fiber, and  $\xi_{\text{core}}$  and  $\xi_{\text{clad}}$  denote the thermo-optic coefficient of fiber

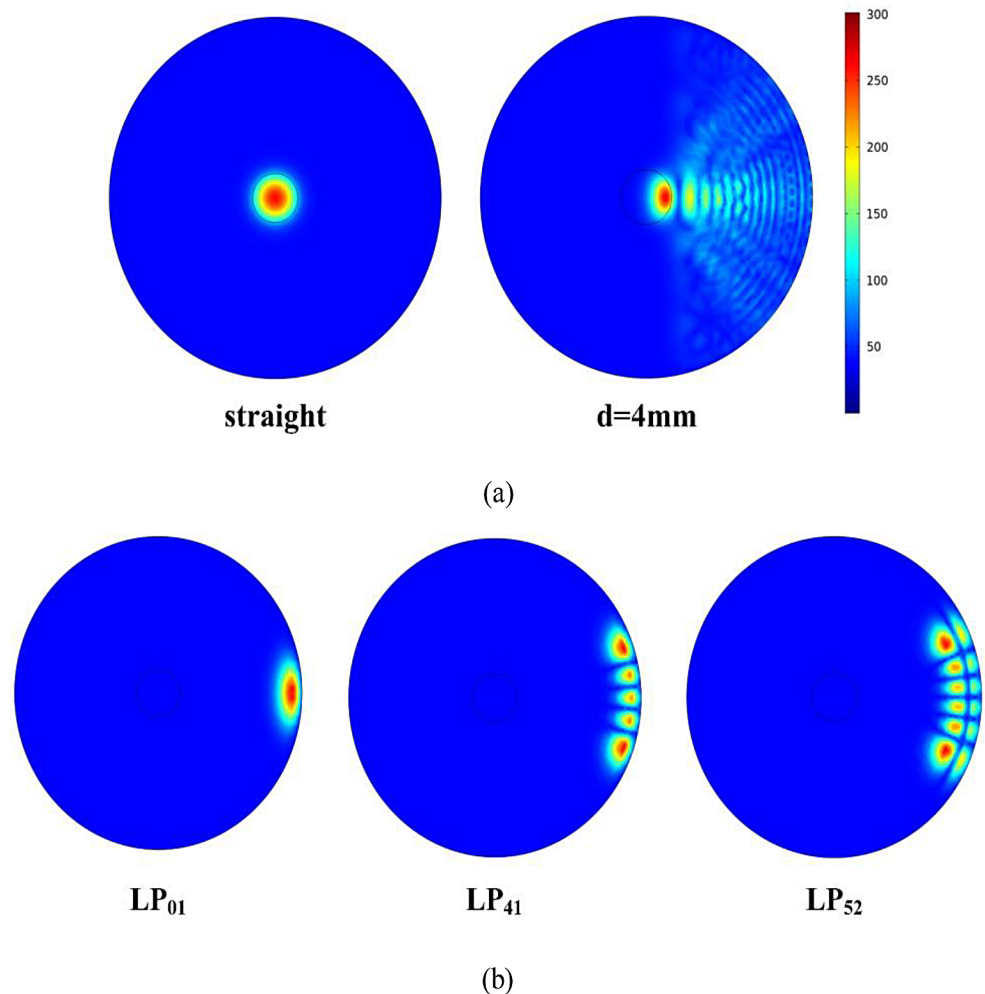
core and cladding, respectively. When the value of  $\Delta n_{\xi}$  is negative and approximately the opposite of  $\frac{\partial\lambda_{\text{dip}}}{\partial T} \approx 0$ , the  $\frac{\partial\lambda_{\text{dip}}}{\partial T} \approx 0$ . This means that the drift of the interference dip with temperature changes is  $\sim 0$ , and the sensor is not sensitive to temperature.

### 2.3 Simulation analysis

Comsol is used to study the effect of curvature on modes field distributions of fiber. The simulation analyses are shown in Fig. 3. By comparing modes field distributions of the straight fiber and the curved fiber with a transverse diameter of 4 mm, it can be found that curvature causes light uniformly distributed in the core to curve sideways and leak into the cladding. The analyses of partial modes field distributions in the fiber cladding are illustrated in Fig. 3(b). The modes listed demonstrate that curvature can make the light transmitted in the cladding excite higher-order modes.

Rsoft is used to analyze normalized energy field distributions of three sensors with different structure. Figure 4(a), (b) and (c) respectively illustrate normalized energy field distributions of the SNFNS straight sensor, the SFS spindle-shaped sensor, and the SNFNS spindle-shaped sensor. In order to compare the differences of the four modes in FMF core intuitively, the lengths of three kinds of fibers are shortened in the simulation. A comparison of Fig. 4(a) and (c) shows that the SNFNS straight sensor does not make the light transmitted in FMF core excite the four modes sufficiently. Meanwhile, due to the increasing of energy leakage caused by curvature, the energy loss of SNFNS

**Fig. 3** The modes field distributions of fiber with different curvature: (a) modes field distributions of the straight fiber and the curved fiber with  $d=4$  mm and (b) modes excited in the cladding of curved fiber with  $d=4$  mm



spindle-shaped sensor is relatively larger. Through the comparison of Fig. 4(b) and (c), it can be found that the period of energy exchange in the SNFNS spindle-shaped sensor is shorter than that of SFS spindle-shaped sensor due to the introduction of NCF. Therefore, at the same length, the modal interferences in the SNFNS spindle-shaped sensor occur more frequently, and the number of interference dips within the corresponding observable range increases.

The fast Fourier transform (FFT) is used to study internal transmission modes of different sensors. The three lines drawn in Fig. 5(a) are FFT analyses of three different schemes respectively, in which the dominate mode in the cladding of the SFS spindle-shaped sensor represented by the blue line is not obvious. Comparing the three lines with different colors, it can be found that the peak value of the dominate mode in the cladding of the SNFNS spindle-shaped sensor is the highest. The higher the peak, the greater the proportion of this mode in interference. By comparing the two lines in Fig. 5(b), it is found that the difference between the peak value of the dominate mode and the weak mode in the cladding of the sensor with  $d=4$  mm is much larger than that of the sensor with  $d=5$  mm, which indicates that the interference process of the

sensor with  $d=4$  mm is more stable. Therefore, it is considered that the SNFNS spindle-shaped sensor with a transverse diameter of 4 mm has better performance from the perspective of FFT analyses of transmission spectra.

### 3 Experimental analysis and discussion

#### 3.1 Experimental apparatuses

As shown in Fig. 6, some experimental apparatuses are applied to study the RI sensing characteristic and temperature sensing characteristic of sensors. These apparatuses mainly include a broadband source (BBS, 1528–1603 nm), an optical spectrum analyzer (OSA, AQ6370D, 600–1700 nm, 0.02 nm), a temperature controller (GDS-50, -20–150°C) and glass plates and so on.

#### 3.2 Experimental process and results analysis

Two sensors with different transverse diameters are made in the experiment, and their specific parameters are plotted in Table 2. The different transmission spectra of the two



**Fig. 4** The normalized energy field distributions of three schemes: (a) SNFNS straight sensor, (b) SFS spindle-shaped sensor and (c) SNFNS spindle-shaped sensor with  $d = 4$  mm

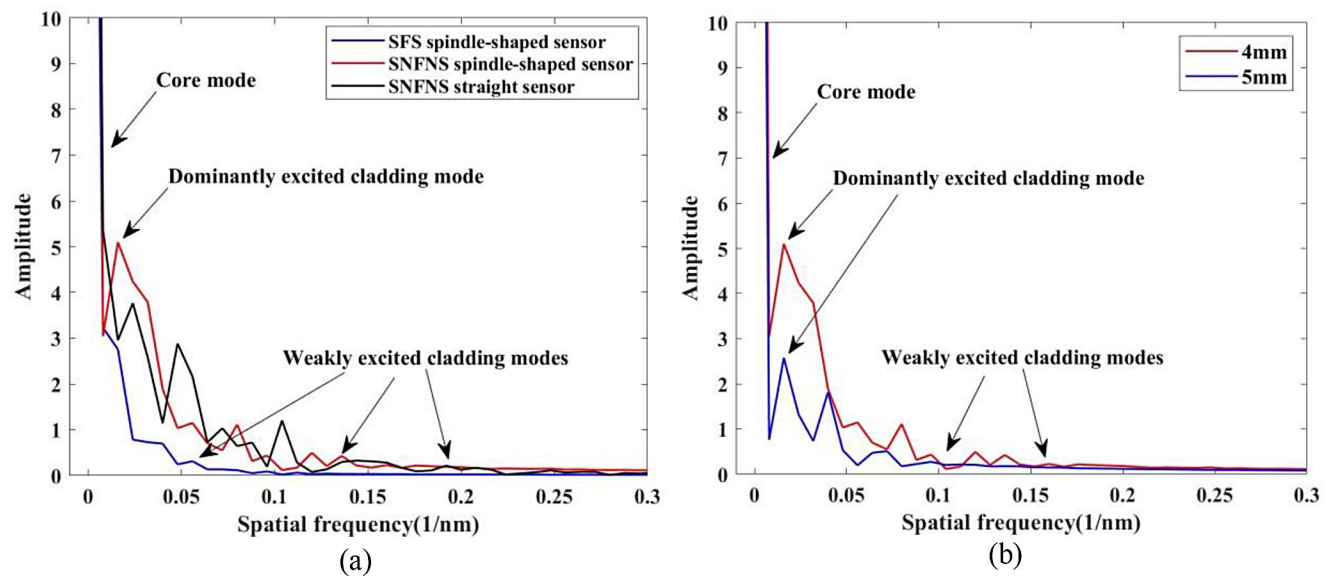
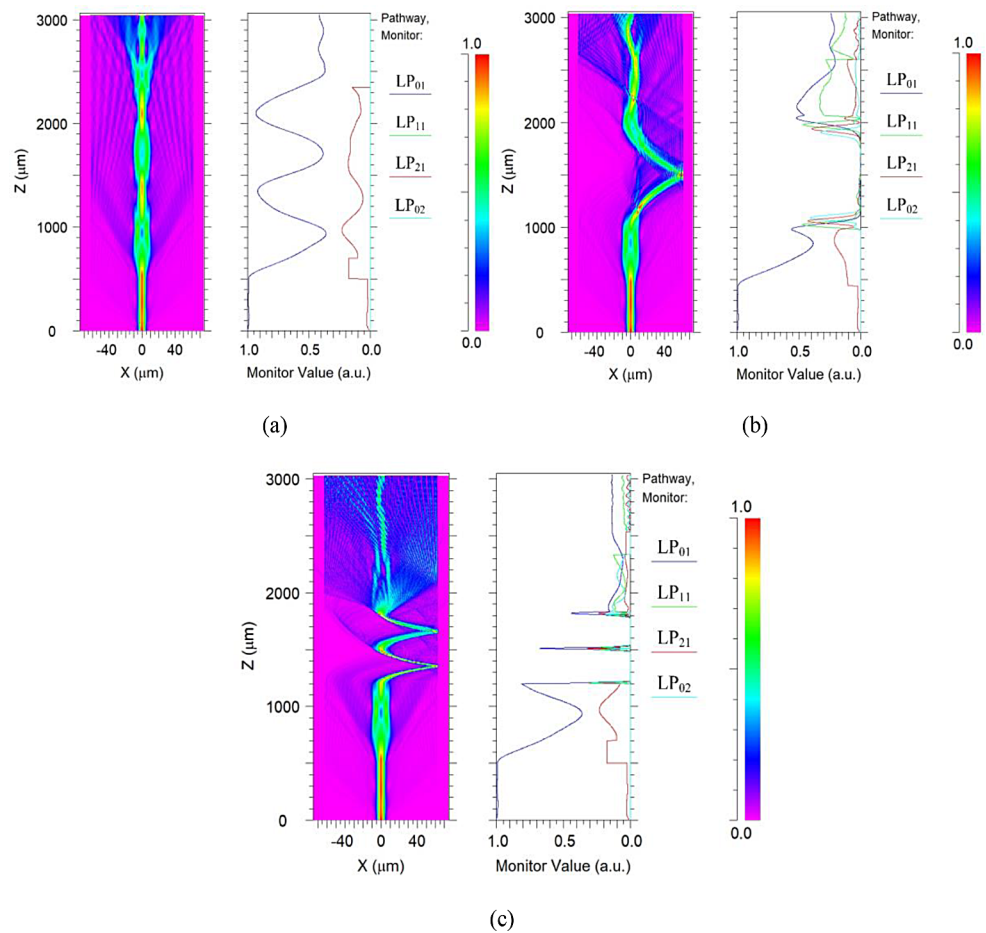


**Fig. 5** The comparison of different spatial frequency spectra: (a) spatial frequency spectra of three schemes (b) spatial frequency spectra of different transverse diameters

sensors are plotted in the Fig. 7. It can be found that with the decreasing of the transverse diameter, the loss of the interference dips also increases. The reduction in transverse diameter increases the curvature of the fiber, leading to an

increase in energy leakage from the fiber, which results in greater losses for a sensor with smaller transverse diameter.

In the RI experiment, glycerin and water are mixed in different proportions to produce solutions of different

**Fig. 6** Sensing experimental apparatuses for refractive index and temperature

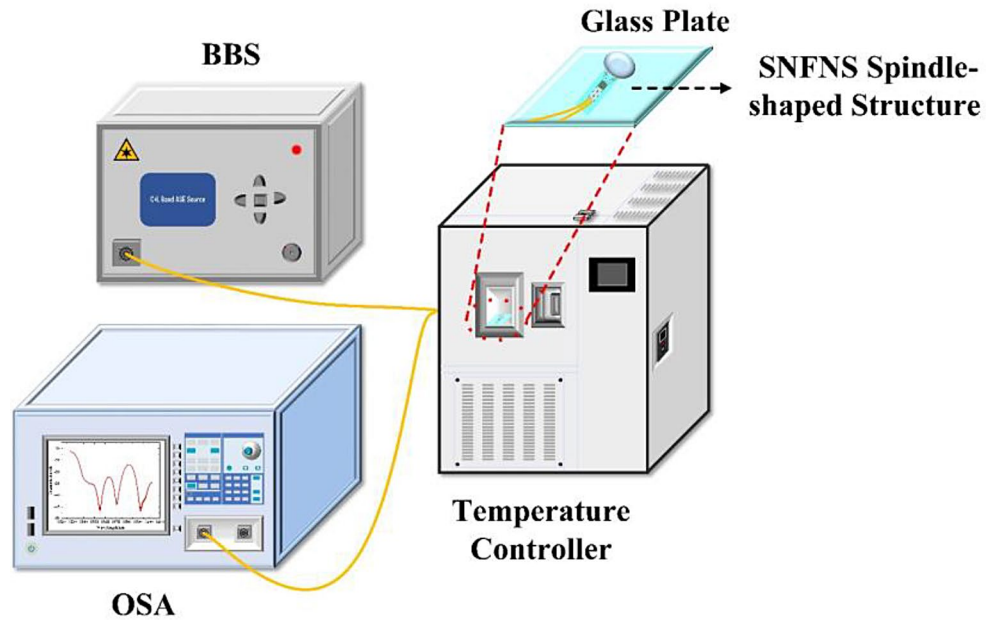


**Table 2** Specific parameters of two sensors

| Sensor sample | $L_1$ (length of NCF) | $L_2$ (length of FMF) | Transverse diameter |
|---------------|-----------------------|-----------------------|---------------------|
| sensor-1      | 2 mm                  | 3 cm                  | 4 mm                |
| sensor-2      | 2 mm                  | 3 cm                  | 5 mm                |

refractive indices (1.333–1.365). The sensors are fixed on glass plates. The configured solutions are dripped onto the sensors in ascending order. The drifts of interference dips are used to analyze the RI characteristics of sensors. It is noteworthy that there could be a little residual solution on the sensor surface when the solution is replaced. There should be sufficient deionized water used to flush out the sensor. The experimental results indicate that all interference dips of two sensors drift towards the long wavelength direction when external RI increases, as shown in Fig. 8. Because

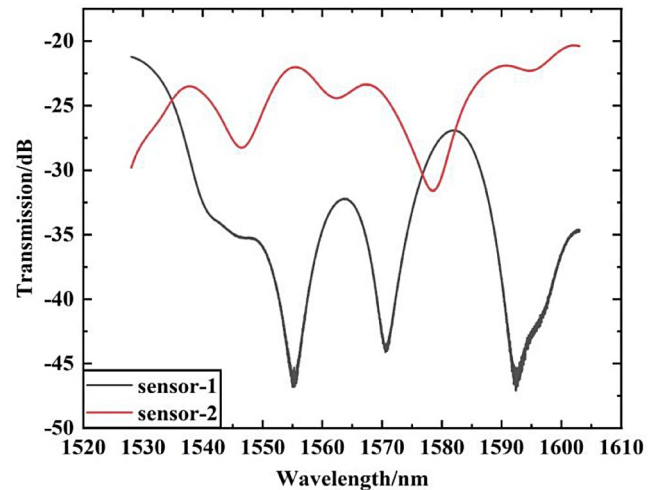


**Fig. 7** Transmission spectra of two sensor samples

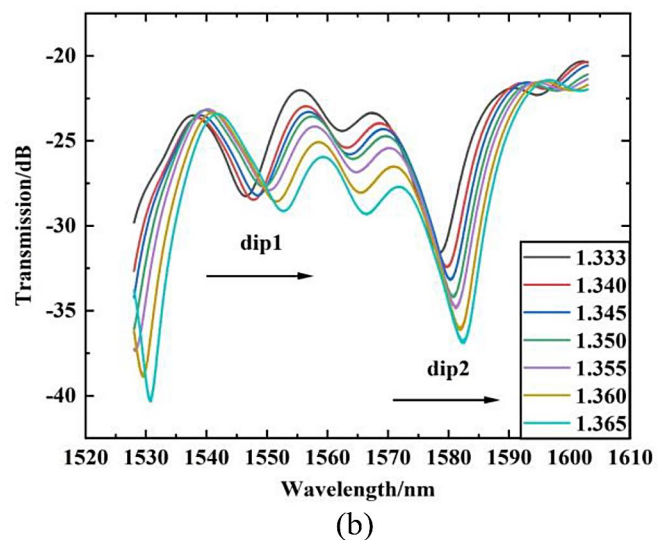
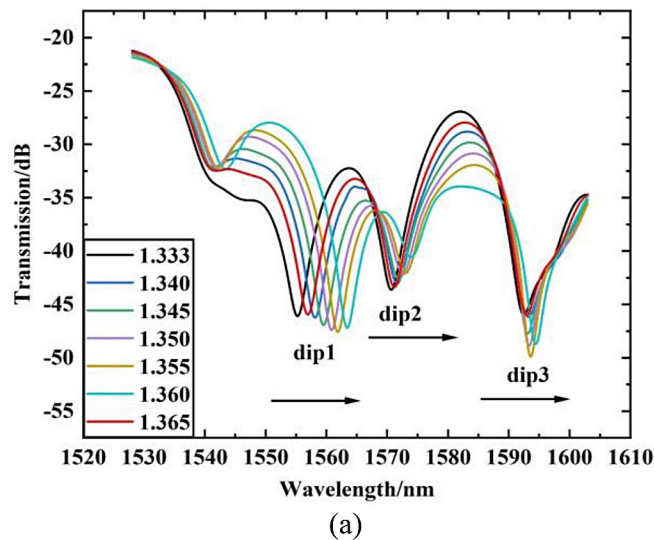


**Fig. 8** Refractive index experiment results of two sensors: (a) transmission spectrum of sensor-1 and (b) transmission spectrum of sensor-2

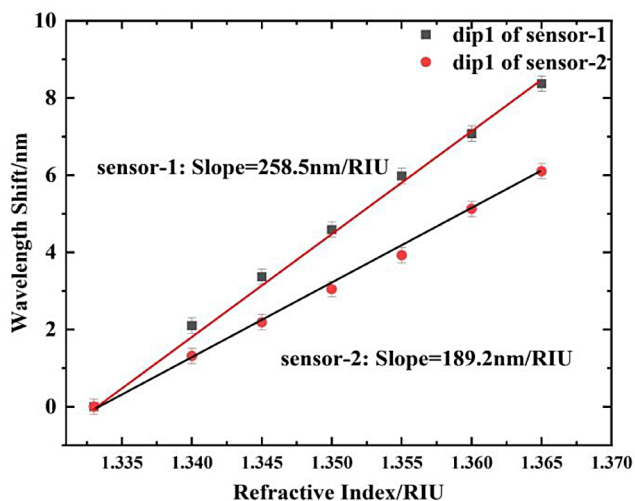


Fig. 9 RI sensitivity comparison of sensors

different interference dips are formed by different modal interferences, these interference dips have different sensing characteristics to the changes of RI. Specifically, these interference dips have different RI sensitivities. The sensitivities of three interference dips of sensor-1 are obtained by calculation as 258.5 nm/RIU with the linear fit of 0.998, 104.7 nm/RIU with the linear fit of 0.993 and 53.3 nm/RIU with the linear fit of 0.997, respectively. And the sensitivities of two interference dips of sensor-2 are 189.2 nm/RIU with the linear fit of 0.997 and 124.0 nm/RIU with the linear fit of 0.995. Comparing the maximum drift of two sensors in Fig. 9, it can be found that the sensor-1 with transverse diameter of 4 mm is more sensitive to RI. This is because

the smaller the transverse diameter, the greater the curvature of the fiber, the more excited higher-order modes of light, making the sensor more sensitive to external changes.

In the temperature experiment, two sensors, whose surface covered with enough deionized water, are placed in a temperature controller, respectively. The starting and ending temperatures are set at 10°C and 70°C, with intervals of 10°C during the period. The drifts of the interference dips are observed and recorded. By analyzing drifts of interference dips with changes in external temperature, the temperature sensing characteristics of sensors can be obtained. The temperature experiment results of two sensors are displayed in Fig. 10. It shows that as the temperature increases from 10°C to 70°C, the drift of interference dips is tiny. For example, the drift of dip1 of sensor-1 is only 0.256 nm. The temperature linear fits of dip1 of two sensors are shown in Fig. 11. On the basis of considering the experimental errors, it can be inferred that the SNFNS spindle-shaped sensor is not sensitive to temperature. This temperature insensitivity characteristic of the sensor can effectively solve the problem of temperature crosstalk.

Stability is one of the most integral performance indicators for judging a sensor. Sensor-1 is placed in solutions of 1.333 and 1.365 for 120 min. The changes in wavelength position of interference dips are plotted in Fig. 12. The drifts of three interference dips are between 0.244 nm and 0.512 nm. Considering the slight errors in the experiment, the sensor is considered stable.

In addition, the polarization effect of the sensor has also been verified. A polarization controller (PC) is connected between the broadband source and the sensor in

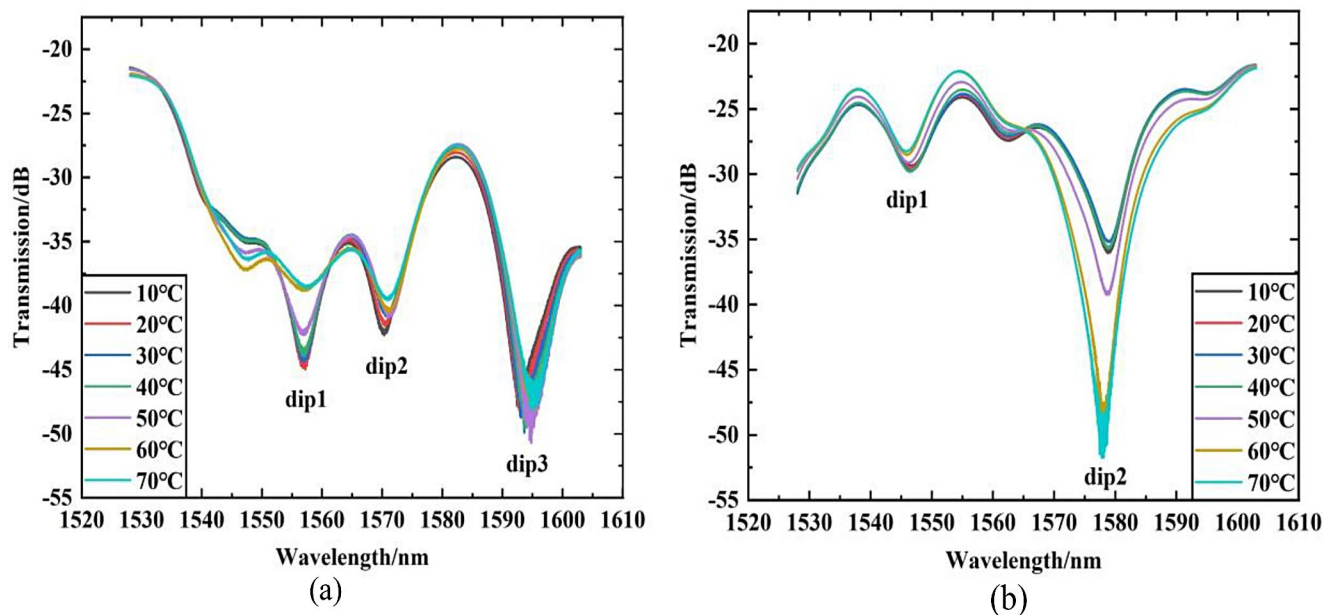


Fig. 10 Temperature experiment results of two sensors: (a) transmission spectrum and linear fit of sensor-1 and (b) transmission spectrum and linear fit of sensor-2

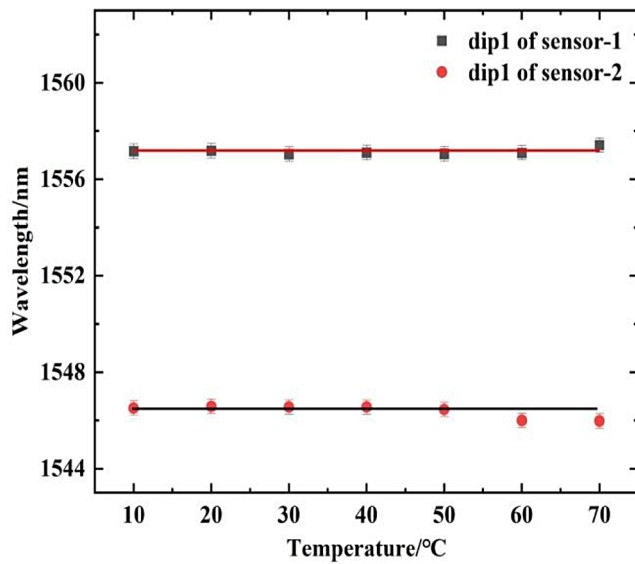


Fig. 11 Temperature linear fits of two sensors

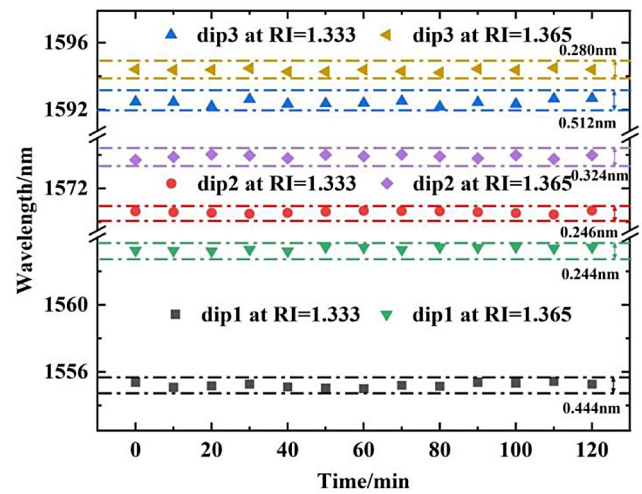


Fig. 12 Stability experiment result of sensor-1

Table 3 Comparison of sensing characteristics with different sensors

| Structure                    | RI sensitivity (nm/RIU) | RI range (RIU) | Temperature sensitivity (nm/°C) | Temperature range (°C) | References |
|------------------------------|-------------------------|----------------|---------------------------------|------------------------|------------|
| D-Shaped sensor Cascaded FBG | -31.79                  | 1.333–1.428    | 0.0287                          | 20–45                  | [7]        |
| Tapered sensor based on PCF  | 263.5                   | 1.3374–1.3477  | -                               | -                      | [18]       |
| Balloon-shaped sensor        | 225.95                  | 1.3493–1.3822  | 0.418                           | 35–60                  | [19]       |
| Tapered MCF sensor           | 171.2                   | 1.3448–1.3774  | -                               | -                      | [23]       |
| SNFNS sensor                 | -134.17                 | 1.333–1.365    | 0.095                           | 30–85                  | [24]       |
| SNFNS spindle-shaped sensor  | 258.5                   | 1.333–1.365    | Insensitivity                   | 10–70                  | This work  |

the experiment. And the PC is rotated at different angles to change the polarization pattern of light in the sensor. It can be observed that the transmission spectrum of the sensor has hardly changed. Therefore, the polarization effect cannot be considered for the proposed sensor.

### 3.3 Discussion

The proposed sensor is compared with other sensors with different structures in Table 3. The refractive index and temperature sensing characteristics of sensors are the main contents of the comparison. It can be considered that the temperature-insensitive SNFNS spindle-shaped sensor has good comprehensive sensing characteristics.

## 4 Conclusion

In this paper, a sensor for refractive index sensitization by curving is presented. The spindle-shaped sensor is formed by curving fibers through a flame based on the SNFNS

structure. The effect of curving on sensor performance is verified through simulation and experiments. The results show that as the transverse diameter decreases, the loss of the sensor increases, and the RI sensitivity also increases. When the transverse diameter is  $\sim 4$  mm, the RI sensitivity of the sensor is 258.5 nm/RIU. At the same time, it is found that the sensor has the characteristic of temperature insensitivity in experiments. Therefore, the potential of this sensor is extraordinary.

**Acknowledgements** This work is supported by Open Projects of State Key Laboratory of Applied Optics (SKLA02020001A02) and National Natural Science Foundation of China (grant number 62003237).

**Author contributions** LJ and ZT guided the experimental research, provided experimental equipment and laboratory, guided and revised the manuscript. ZY mainly conducted experimental research and wrote manuscript text, and processed all experimental data. HZ made corrections to the manuscript. PT and LM assisted in the operation of the experiment.

**Data availability** No datasets were generated or analysed during the current study.



## Declarations

**Competing interests** The authors declare no competing interests.

## References

- R.X. Liu, X. Zhang, X.S. Zhu, Y.W. Shi, Optical fiber hydrogen sensor based on the EVA/Pd coated hollow fiber. *IEEE Photon J.* **14**(3), 6825806 (2022)
- Q. Wang, B.T. Wang, L.X. Kong, Y. Zhao, Comparative analyses of bi-tapered fiber mach-Zehnder interferometer for refractive index sensing. *IEEE Trans. Instrum. Meas.* **66**(9), 2483–2489 (2017)
- T. Okazaki, H. Kamio, M. Yoshioka, A. Ueda, H. Kuramitz, T. Watanabe, U-shaped plastic optical fiber sensor for scale deposition in hot spring water. *Anal. Sci.* **38**, 1549–1554 (2022)
- W.H. Zhang, M. Wu, L. Jing, Z.R. Tong, P. Li, M.Y. Dong, X. Tian, G.X. Yan, Research on in-line MZI optical fiber salinity sensor based on few-mode fiber with core-offset structure. *Measurement.* **202**, 111857 (2022)
- X.P. Zhang, W. Peng, Y. Liu, Q.X. Yu, Core-offset-based fiber Bragg grating sensor for refractive index and temperature measurement. *Opt. Eng.* **52**(2), 024402 (2013)
- Y. Zhao, M.Q. Chen, F. Xia, H.F. Hu, Spectrum online-tunable Mach-Zehnder interferometer based on step-like tapers and its refractive index sensing characteristics. *Opt. Commun.* **403**, 143–149 (2017)
- Y. Dong, S.Y. Xiao, B.L. Wu, H. Xiao, S.S. Jian, Refractive index and temperature sensor based on D-shaped fiber combined with a fiber Bragg grating. *IEEE Sens. J.* **19**(4), 1362–1367 (2019)
- M.Y. Chen, G.F. Xu, X.Q. Su, T. Zhou, Y. Liang, T.Y. Gong, A temperature insensitive strain sensor based on SMF-FMF-NCF-FMF-SMF with core-offset fusion. *Appl. Phys. B* **130**, 5 (2024)
- J.H. Guo, S.P. Lian, Y. Zhang, Y.F. Zhang, D.Z. Liang, Y.Q. Yu, R.H. Chen, C.L. Du, S.C. Ruan, High-temperature measurement of a fiber probe sensor based on the Michelson interferometer. *Sensors.* **22**(1), 289 (2022)
- L.L. Li, Y. Wei, W.L. Tan, Y.H. Zhang, C.L. Liu, Z. Ran, Y.X. Tang, Y.D. Su, Z.H. Liu, Y. Zhang, Fiber cladding SPR sensor based on V-groove structure. *Opt. Commun.* **526**, 128944 (2023)
- Z.J. Rui, Z.H. Xiang, F. Zeng, C.P. Lu, Y.F. Wang, T. Geng, W.M. Sun, L. Yuan, Liquid level sensor with high sensitivity based on hetero core structure. *IEEE Sens. J.* **22**(14), 14051–14057 (2022)
- S. Zhang, Z.M. Wang, M.Y. Zhu, L. Li, S.J. Wang, S. Li, F. Peng, H.W. Niu, X. Li, S.F. Deng, T. Geng, W.L. Yang, L.B. Yuan, A compact refractive index sensor with high sensitivity based on multimode interference. *Sens. Actuators A* **315**, 112360 (2020)
- C.X. Teng, F.D. Yu, S.J. Deng, H.Q. Liu, L.B. Yuan, J. Zheng, Deng., Displacement sensor based on a small U-shaped single-mode fiber. *Sensors.* **19**(11), 2531 (2019)
- A.A. Silva, L.A.M. Barea, D.H. Spadoti, C.A.D. Francisco, Hollow-core negative curvature fibers for application in optical gas sensors. *Opt. Eng.* **58**(7), 072011 (2019)
- V. Ahsani, F. Ahmed, M.B.G. Jun, C. Bradley, Tapered fiber-optic Mach-Zehnder interferometer for ultra-high sensitivity measurement of refractive index. *Sensors.* **19**(7), 1652 (2019)
- X.P. Zhang, W. Peng, Fiber optic refractometer based on leaky-mode interference of bent fiber. *IEEE Photon Technol. Lett.* **27**(1), 11–14 (2015)
- J.P. Liu, X.D. Zhang, J.R. Yang, J. Kang, X.F. Wang, Common difference temperature compensation based fiber refractive index sensor through asymmetrical core-offset splicing. *Opt. Commun.* **427**, 261–265 (2018)
- P. Gao, Y.P. Gao, M.Y. Li, S.W. Liu, Y.N. Zhang, All-fiber mach-Zehnder interferometer with dual-waist PCF structure for highly sensitive refractive index sensing. *Appl. Phys. B* **125**, 107 (2019)
- X. Liu, Y. Zhao, R.Q. Lv, Q. Wang, High sensitivity balloon-like interferometer for refractive index and temperature measurement. *IEEE Photon Technol. Lett.* **28**(13), 1485–1488 (2016)
- B.C. Wu, H.Y. Bao, Y.F. Zhou, Y. Liu, J. Zheng, Temperature dependence of a refractive index sensor based on a bent core-offset in-line fiber mach-Zehnder interferometer. *Opt. Fiber Technol.* **67**, 102748 (2021)
- X.P. Zhang, L.X. Xie, Y. Zhang, W. Peng, Optimization of long-period grating-based refractive index sensor by bent-fiber interference. *Appl. Opt.* **54**(31), 9152–9156 (2015)
- H.M. Luo, X.W. Li, W.W. Zou, X. Li, Z.H. Hong, J.P. Chen, Temperature-insensitive microdisplacement sensor based on locally bent microfiber taper modal interferometer. *IEEE Photon J.* **4**(3), 772–778 (2012)
- C.B. Zhang, T.G. Ning, J. Li, L. Pei, C. Li, H. Lin, Refractive index sensor based on tapered multicore fiber. *Opt. Fiber Technol.* **33**, 71–76 (2017)
- M. Wu, W.H. Zhang, Z.R. Tong, X. Wang, Y.M. Zhao, J.T. Zhang, G.X. Yan, Mach-Zehnder interferometer for multi-parameter measurement sensor based on SMF-NCF-FMF-NCF-SMF, *Optik*, 249, 168227 (2022)

Springer Nature or its licensor (e.g. a society or other partner) holds exclusive rights to this article under a publishing agreement with the author(s) or other rightsholder(s); author self-archiving of the accepted manuscript version of this article is solely governed by the terms of such publishing agreement and applicable law.